Photocatalytic decolorization of ZnO/Fe for the removal of methylene blue by new microwave methodology

Yonrapach Areerob[1], Won-Chun Oh[2,3], and Kongsak Pattarith[4,*]

[1] Department of Industrial Engineering, School of Engineering, King Mongkut's Institute of Technology Ladkrabang, Bangkok 10520, Thailand

[2] Department of Advanced Materials Science & Engineering, Hanseo University, Seosan-si, Chungcheongnam-do 31962, South Korea

[3] Anhui International Joint Research Center for Nano Carbon-Based Materials and Environmental Health, College of Materials Science and Engineering, Anhui University of Science & Technology, Huainan 232001, People's Republic of China

[4] Department of Chemistry, Faculty of Science, Buriram Rajabhat University, Buriram 31000, Thailand

ABSTRACT

The photocatalysis of ZnO/Fe was performed by the simple microwave method for the removal of methylene blue. All samples were found to possess a single-phase monoclinic scheelite structure. On loading 5.0 mol% of Fe to the samples, the photocatalytic activities were enhanced, suggesting the potential application of the material as a superior visible light-driven photocatalyst relative to pure ZnO for the decolorization of methylene blue dye. The enhanced decolorization activity of the photocatalyst demonstrated the ability of Fe to reduce the band gap energy of ZnO and improve the electron transfer in the ZnO/Fe adsorbent. Moreover, the ultraviolet–visible absorption experiments exhibited an excellent decolorization rate (30 min) along with a decolorization efficiency of 93% upon the UV irradiation of ZnO/Fe in the pH range. The possible reaction mechanism and decolorization pathway of the photocatalyst were discussed in detail, and the stability of the catalyst was confirmed by the reusability test.

1 Introduction

With the exponential growth of the industrial sector in Thailand and around the world, industrial pollution, such as the contamination of water by toxins and dyes, is seriously affecting the aquatic animals and human life on earth. Nearly 200,000 tons of over 10,000 different dyes were let into wastewater effluents after the batch processes followed in the textile industries [1]. Water contamination can be found on the surface as well as groundwater due to the presence of highly common organic toxins such as crystal violet (CV), methyl orange (MO), and methylene blue (MB). The MB dye poses adverse health and environmental effects due to its frequent use in silk and cotton fabrics, causing nausea, eye irritation, cyanosis, and respiratory diseases in both humans and aquatic organisms [2, 3]. Therefore, it is necessary to

Springer

remove these dyes from industrial wastewater before discharging them in order to protect the environment and lives. Many conventional treatment processes, including decoloration, biodegradation, ozonation, physical systems like adsorption and photocatalytic decolorization were employed for this purpose [4]. Among them, the photocatalytic remediation and adsorption of dyes using photocatalyst is the most preferred choice for the treatment of pollutants in wastewater due to its simplicity, efficiency, economic viability, non-toxicity, and sustainability [5].

Recently, researchers have been focusing on the development of nanoparticle-based adsorbents, such as metal oxide nanoparticles (NPs), carbon-based, and polymer NPs to improve the dye removal efficacy in wastewater [6]. Among various metal oxides, zinc oxide (ZnO) is the most common photocatalyst used for decolorization due to its unique properties of high photocatalytic activity, low quantum yield, wide band gap (3.3 eV), low conductivity, toxicity, recombination rate, and high surface area.

Moreover, ZnO act as forceful metal oxide, which can generate electrons and holes in the presence of light to perform excellent dye decolorization depending on their bandgap. ZnO semiconductor has consideration for many usages and on doping with metallic elements, ZnO properties were reformed by tuning size and bandgap. Transition metal Iron (Fe) was preferred as dopant due to the convenience of d electrons at t_{2g} level can join the ZnO valance bond. When the results of ZnO doped with Mo, Cu, Ni, and Co [7–9] transition metals, Fe-doped ZnO semiconductor supports in oxidation and reduction to lessen the hazardous of dye by enhancing photocatalytic activity properties with optimized dopant concentration under visible light irradiation. We prefer on Fe-doped ZnO nano-photocatalyst, owing to scarce reports on Fe-doped ZnO adapts high and low photocatalytic activity compared to ZnO.

It has been reported in literature that photocatalytic efficiency is dependent upon band gap and increases with decrease in band gap. P. Hemalatha and co-worker were synthesized Lanthanum-doped ZnO flower-like structured nanoparticles as photocatalyst through microwave assisted sol–gel technique for degrade methylene blue under UV light irradiation. They reported that degradation efficiency under UV light irradiation was 90% for 0.5 mol% La [10]. A. Modwi et al. [11] reduced the band gap of ZnO while inducing copper in combination with transition metals for enhancing photocatalytic properties. They achieved band gap reduction by 6.35% with copper doping. Moreover, they found that The Ag/Cu/ZnO photo-composite system showed considerably enhanced photodegradation up to 83% for malachite green (MG) under visible light illumination.

Selvaraj et al. [12] synthesized binary Gd-doped ZnO nanocomposites with the aim to enhance the decolorization activity of methylene blue under visible light. The results demonstrated the improved visible light absorption of the materials due to the incorporation of Gd ions into the ZnO lattice. Recently, Zhang et al. [13] reported that the doping of Mo on TiO_2 powders was found to induce a visible shift and hence result in enhanced absorption under visible light. The enhancement of the photocatalytic efficiency was increased up to 93% due to the role of metals as electron traps, thus promoting the electron–hole separation and interfacial charge-transfer process from the catalyst to the adsorbed substrate. However, most of these metals are very expensive. Among them, the addition of Fe (iron) has gained much interest due to the influence of half-filled d-orbital, which is considered to have a great impact on the photocatalytic activity of ZnO [14, 15].

In the present work, a facile microwave method was employed to synthesize Fe-doped ZnO. The photocatalytic activities of ZnO and 5.0 mol% of Fe-loaded ZnO were evaluated for the photooxidation of various concentrations of methylene blue (MB) in the range of 10–50 ppm under visible light irradiation. Moreover, the optimum amount of ZnO/Fe (0.1–0.5 g), pH of the MB solutions (3–9), and reusability of the ZnO/Fe adsorbents were investigated. The possible reaction mechanism for the MB dye decolorization process and characteristics of ZnO are discussed in detail.

2 Experimental

2.1 Materials

Analytical grade Zinc Oxide (CAS No. 1314-13-2, 99% purity), iron (III) chloride hexahydrate [$FeCl_3.6H_2O$, CAS No. 10025-77-1 (ACS reagent, 97%)], methylene blue [$C_{16}H_{18}ClN_3S$, CAS No. 122965-43-9, (analytical purity $\geq$ 98.0%)], ethanol (anhydrous, $\geq$ 99.5%), and deionized (DI) water were purchased from Sigma-

Aldrich company, and used without any additional purification.

2.2 Sample preparation

The microwave method was employed to synthesize the ZnO/Fe photocatalysts [16]. Firstly, 10 g of ZnO was dissolved in 100 mL of DI water and stirred for 30 min at room temperature. To the above mixture, 0.103 g of $FeCl_3.6H_2O$ was added, and the solution was placed in the microwave equipment at 800 watts for 30 min. The solutions were cooled down to room temperature. Finally, the mixture was washed thoroughly with water and centrifuged at 5000 rpm for 10 min. Furthermore, it was dried at 100 °C for 12 h. The photocatalysts were stored in an opaque container and stored in a desiccant bowl for further studies. The schematic diagram for the preparation of ZnO/Fe is shown in Fig. 1.

2.3 Characterization of the sample

The crystalline ZnO/Fe photocatalyst was analyzed using the powder X-ray diffractometer (Cu Kα–1.545 Å). The structural and morphological properties of ZnO/Fe were investigated by transmission electron microscopy (TEM). The FT-IR (Spectrum Two/L1101040, PerkinElmer) spectra were recorded in the wavelength range of 400–4000 cm^{-1} to characterize the functional groups. The quantitative determination of MB was performed at a wavelength of 664 nm using the UV–Vis spectrophotometer, SHIMADZU (SHIMADZU Corporation).

2.4 Photocatalytic activity studies

Various concentrations of methylene blue (MB) (10, 20, 30, 40, and 50 mg L^{-1}) in 100 mL were used to evaluate the photocatalytic efficiency of pure ZnO and ZnO/Fe powders. The MB dye concentration was measured using the double beams spectrophotometer at regular time intervals at the maximum wavelength of the MB dye absorption (664 nm). The MB solution treated with the ZnO/Fe photocatalyst was stirred for 30 min in the dark to enhance the adsorption and desorption equilibrium on the surface of the material. Later, the pH of the mixing solution was optimized in the range of 3–9. Furthermore, the mixture solution was exposed to visible light for the initiation of the photocatalytic activity, and the dye

solution was taken every 5 min and centrifuged at 3000 rpm for 10 min. The decolorization efficiency was calculated using the following equation:

$$\text{Decolorization rate}\,(\%) = \frac{(C_0 - C)}{C} \times 100\%, \qquad (1)$$

where C_0 represents the initial concentration of MB before irradiation and C is the concentration of MB after light irradiation at a time (t) [17].

2.5 Reusability

The ZnO/Fe photocatalyst was added to 10 mg L^{-1} of MB solution under continuous stirring for 30 min. About 1 mL of the sample was withdrawn from the tubes every 5 min for a period of 30 min, and the catalyst was removed from the sample by centrifugation at 5000 rpm for 10 min. The concentrations of the MB dye solution at different reaction times were compared with the initial concentrations of the dye to determine the decomposition rate. After 30 min of the experiment, the remaining solution was filtered using a decompression filter to separate the catalyst. The separated catalyst was washed thoroughly with distilled water and dried at 110 °C for 3 h. The ZnO/Fe photocatalyst was reused to perform the same experiment thrice.

3 Results and discussion

3.1 XRD analysis

The powder XRD diffraction patterns of ZnO/Fe [(a) red line] and pure ZnO [(b) blue line] photocatalysts are shown in Fig. 2. From the diffraction pattern, it was observed that the diffraction peaks corresponding to ZnO matched well with the standard JCPDS card no (36–1451). The obtained XRD peaks at the 2θ values of 31.76°, 34.43°, 36.27°, and 47.54° were assigned to the (100), (002), (101), and (102) planes, respectively. The diffraction peaks of the Fe-loaded ZnO were quite broader than pure ZnO, suggesting the presence of smaller crystallites upon loading iron [18]. However, the added Fe did not penetrate the crystalline chromatography of the ZnO peak, as indicated by the constant X-ray diffraction pattern. Therefore, the presence of Fe needs to be confirmed by employing another technique.
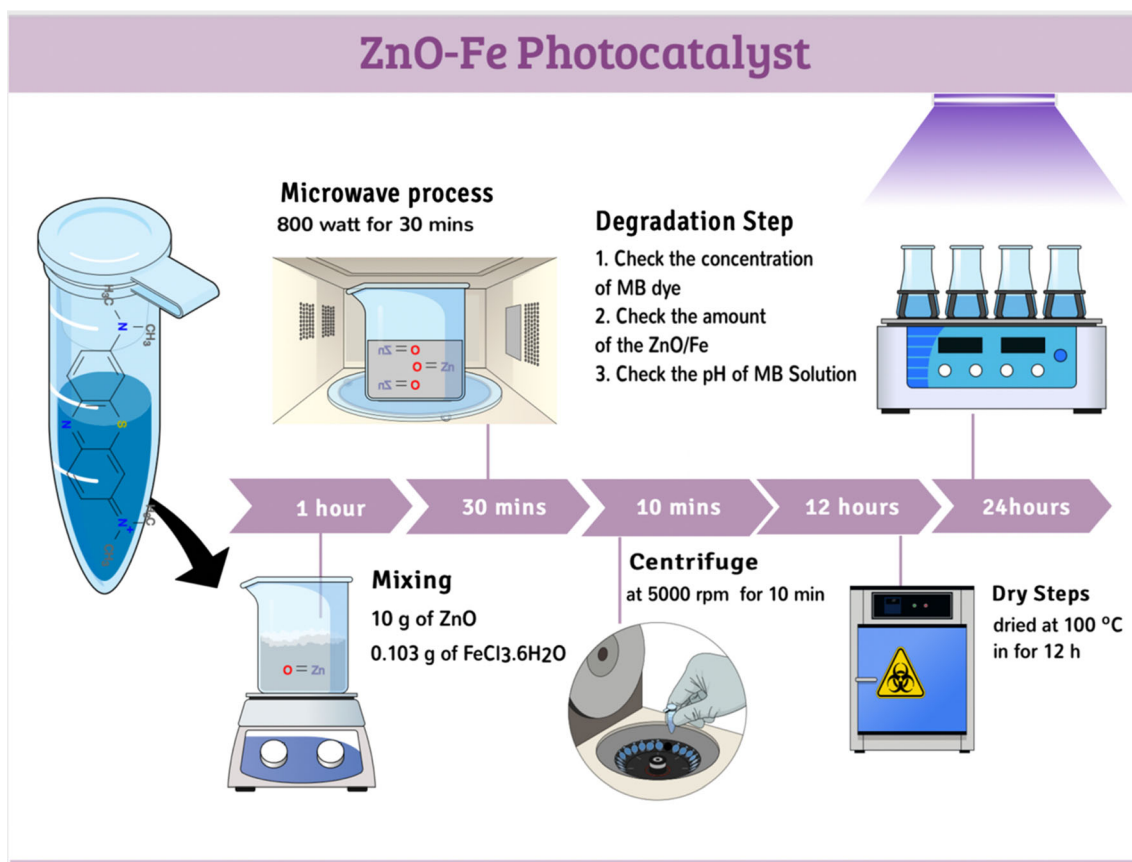
Fig. 1 The schematic diagram for the synthesis of ZnO/Fe
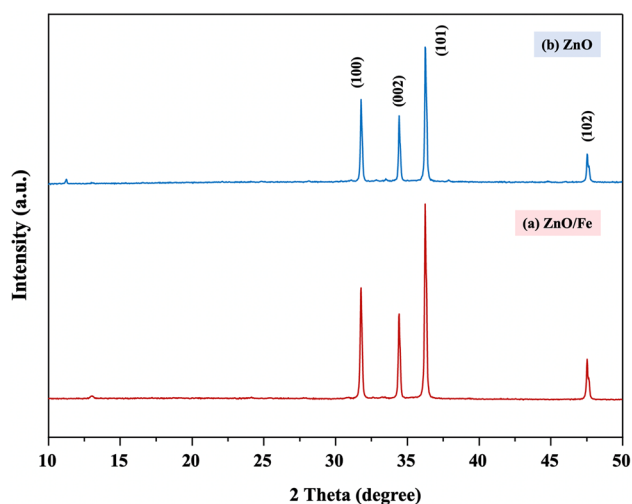
Fig. 2 X-ray diffractograms of **a** ZnO/Fe and **b** ZnO (Color figure online)

3.2 FT-IR spectrometry

The synthesis of ZnO and ZnO/Fe using natural honey was examined by Fourier Transform-Infrared spectroscopy (FT-IR), as shown in Fig. 3a, b. Generally, the absorption bands of the metal oxides are detected in the wavelength of 1000–400 cm^{-1} due to their inter-atomic vibrations. From the spectrum in Fig. 3a, the main absorption bands at 720.72, 832.84, 990.15, 1218.17, 1379.82, 1508.83, 1732.14, 3372.86 cm^{-1} were assigned to the vibrations of the Zn–O bond. The broad absorption band displayed in Fig. 3b at 3436 cm^{-1} was assigned to the –OH bond of the surface-adsorbed H$_2$O molecule. Apart from the distinct peak of Zn–O, weak absorption peaks were observed at 715 cm^{-1} attributed to the characteristic Fe–O stretching mode [19]. In addition, the Zn–O vibration mode was not detected due to its occurrence at a wavelength of approximately 533 cm^{-1}.

3.3 Morphological and chemical state characterization

The morphology of ZnO/Fe was analyzed by TEM, as shown in Fig. 4a, b, respectively. From Fig. 4a, b,

Fig. 3 Infrared spectra of ZnO and ZnO/Fe
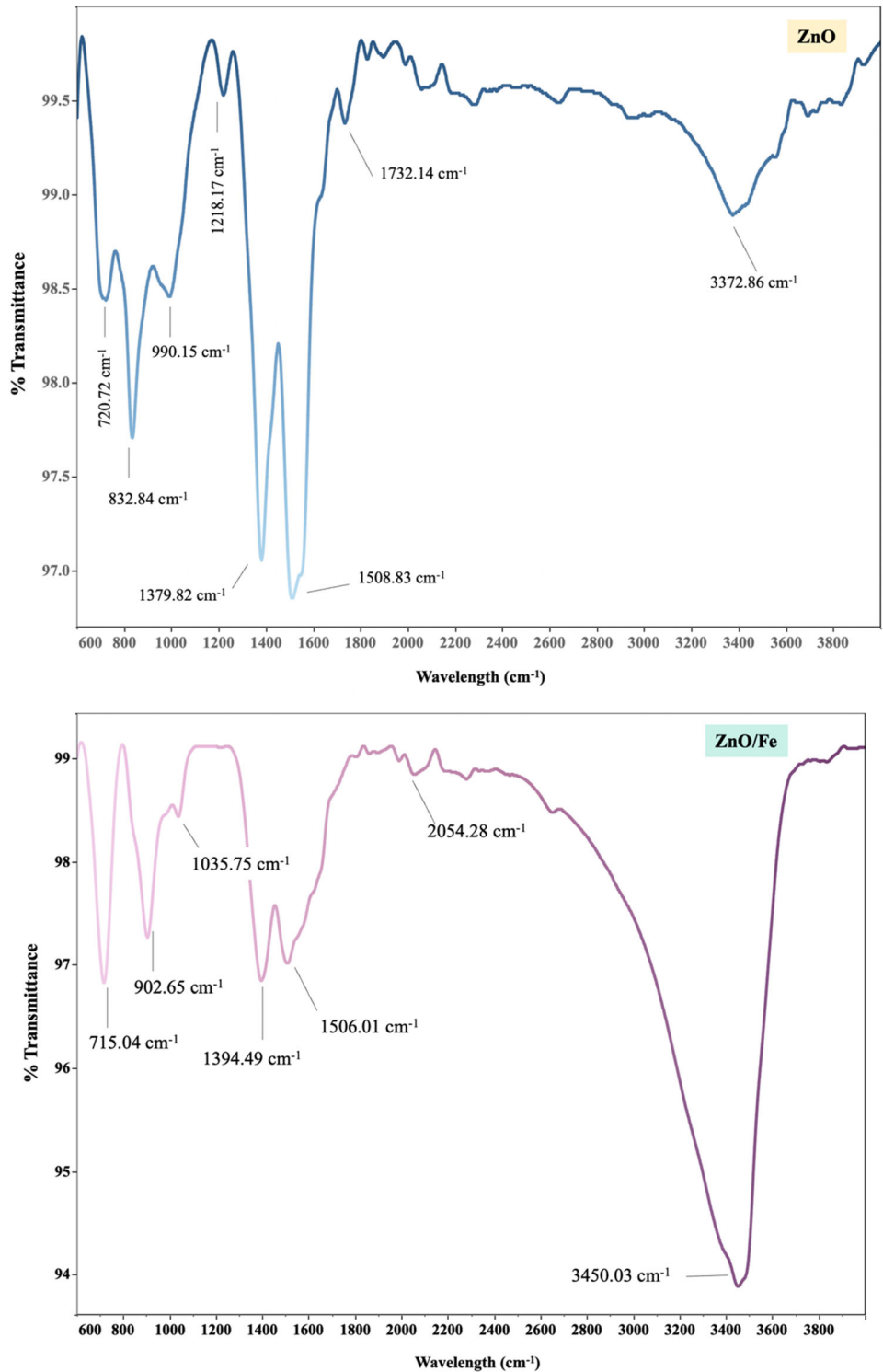
the larger ZnO particles were clearly demonstrated with an average particle size of about 0.3 μm, and the small Fe particles were clearly adhered to the surface, confirming the penetration of the surface. The iron particles were found to be distributed over the surface of ZnO, instigating a positive effect on the adsorption and photocatalytic processes.

The element constitution and the chemical states of ZnO/Fe were also investigated by XPS spectra as shown in Fig. 5. In the Fig. 5a, the O 1s peak is fitted
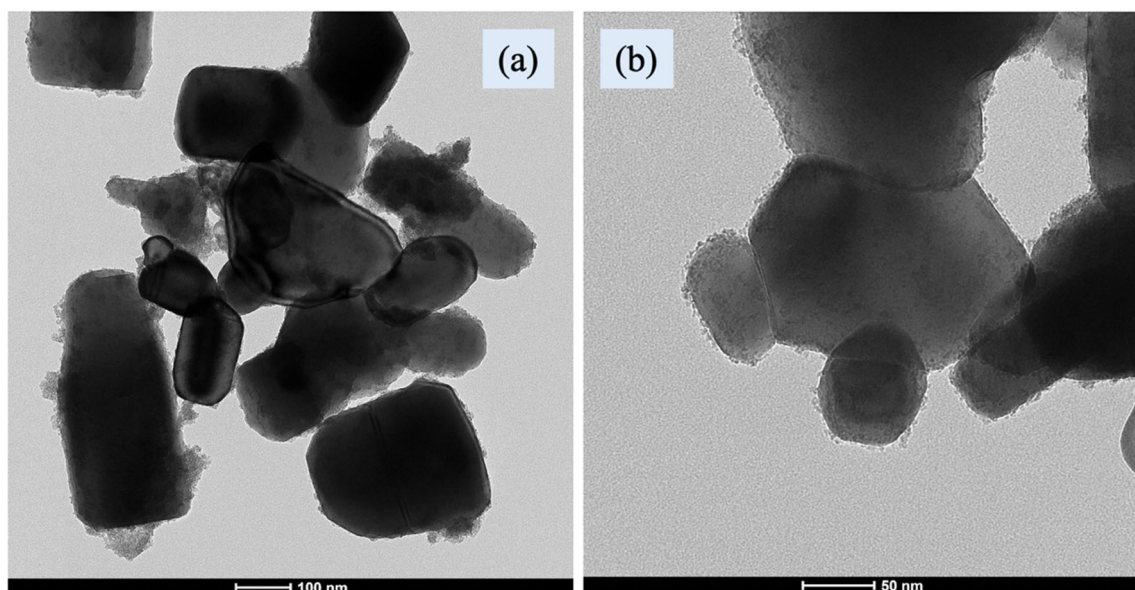
Fig. 4 TEM images of ZnO/Fe (**a** and **b**)

into two peaks located at 532.55 eV and 537.34 eV, indicating the presence of two kinds of O species in the ZnO/Fe, which are attributed to the oxygen vacancy (O_V), and chemisorbed oxygen of the surface hydroxyls (O_C). The XPS of Fe $2p$ is shown in Fig. 5b, the peaks of Fe $2p_{3/2}$ and Fe $2p_{1/2}$ are at 710.1 eV and 723.1 eV, which is suggesting the presence of Fe^{2+} in the ZnO/Fe composites. The appearance of Fe^{2+} is attributed to the presence of Ov in ZnO lattice with requirement of electrical neutrality. Moreover, high-resolution XPS spectra of Zn shown in Fig. 5c shows the two strong peaks located at 1027.03 eV and 1052.11 eV can be indexed to the binding energies of Zn $2p_{3/2}$ and Zn $2p_{1/2}$, respectively, indicating Zn existing in form of Zn^{2+} [20, 21].

3.4 UV–visible spectral analysis

Figure 6 illustrates the UV–visible diffuse reflectance spectra of the pure ZnO and ZnO/Fe catalysts. Pure ZnO catalyst with the monodispersed spherical is a white colored powder having an absorption cut off edge at 395 nm. The absorption spectra of Fe-loaded ZnO showed higher absorption of ultraviolet radiation. Also, the addition of Fe was found to induce a redshift of the ZnO absorption spectrum, which may

be attributed to the charge carrier transfer mobility between Fe and the conduction band of ZnO [22].

The band gap energy of ZnO/Fe was determined on the basis of its absorption spectrum according to the following Tauc plot and Kubelka–Munk function equation $[F(R)\ E]^2$:

$$(\alpha h v) = A\big(h v - E_g\big)^n, \tag{2}$$

$$F(R)E^2 = \left(\frac{1 - R^2}{2R} \times h v\right)^2, \tag{3}$$

where α, v, E_g, and A are the absorption coefficient, frequency of the light, band gap, and a constant, respectively [23]. n is a coefficient (n = 1/2 for direct band gap material). The band gap value of ZnO was 3.95 eV, while ZnO/Fe exhibited the band gap value of 3.72 eV (Fig. 7). The band gap energy was decreased upon the addition of Fe due to the influence of Fe particles on electron–hole pairs under visible light irradiation.

3.5 Surface and particle analysis

BET surface area of ZnO and ZnO/Fe photocatalyst (presented in Fig. 8 and inset image) has been determined as 13.25 (pore diameter 3.25 Å) and 25.57 $m^2\ g^{-1}$ (pore diameter 2.54 Å) for ZnO and ZnO/Fe which is sufficient enough to provide active sites for
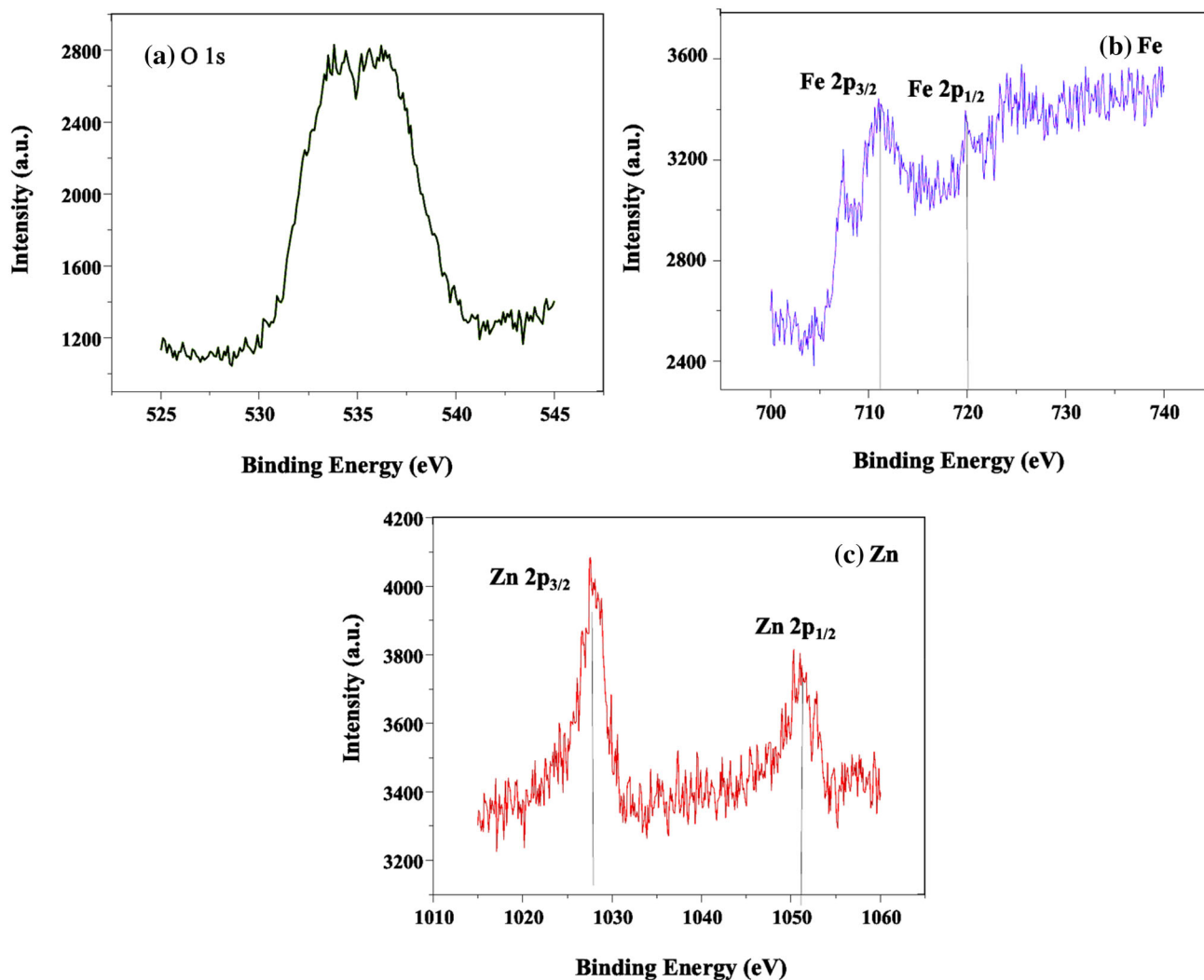
Fig. 5 XPS high-resolution spectra of **a** O 1*s*, **b** Fe 2*p*, and **c** Zn 2*p*

taking place the photocatalytic reactions onto nanocomposite material and it can confirm that after combined with Fe, which can improve the surface area. N_2 adsorption–desorption curve closely matches with IUPAC Type III isotherm, suggesting the photocatalyst's macro-porous nature [24].

Moreover, Fig. 9 shows the particle diameter distribution of ZnO and ZnO/Fe photocatalyst, in all the cases, the observed distribution was normal and monomodal. For ZnO, we observed a particle diameter range of 600–1000 nm and the particle diameter average about 904 nm. However, for the ZnO/Fe we observed a particle diameter represents about 275 nm, with most of the particles in the finest size distribution and the particle diameter average about 717 nm with most of the particles in the finest size distribution. Therefore, it can confirm that after ZnO combined with Fe observed might be attributed to the different size distributions.

3.6 Photocatalytic activity toward methylene blue (MB) decolorization

The factors affecting the optical catalytic process of the removal of MB dye, such as concentration of MB dye solution, amount of ZnO/Fe photocatalyst, and pH of the MB solutions, were studied by the microwave treatment.

Fig. 6 Reflectance-wavelength spectra of pure ZnO and ZnO/Fe
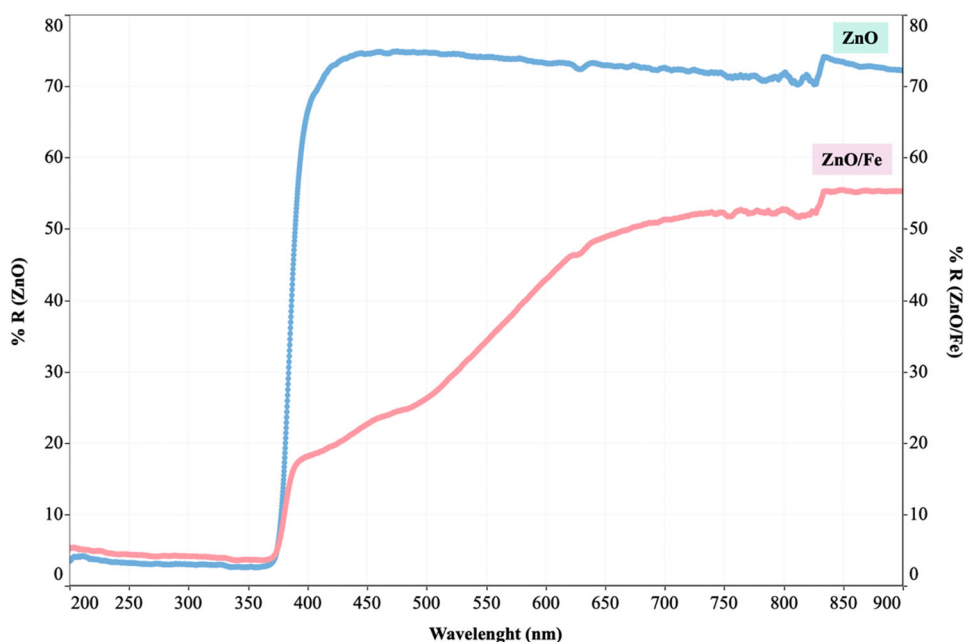
**Fig. 7** Tauc's plots for ZnO and ZnO/Fe obtained using the Kubelka-Munk function
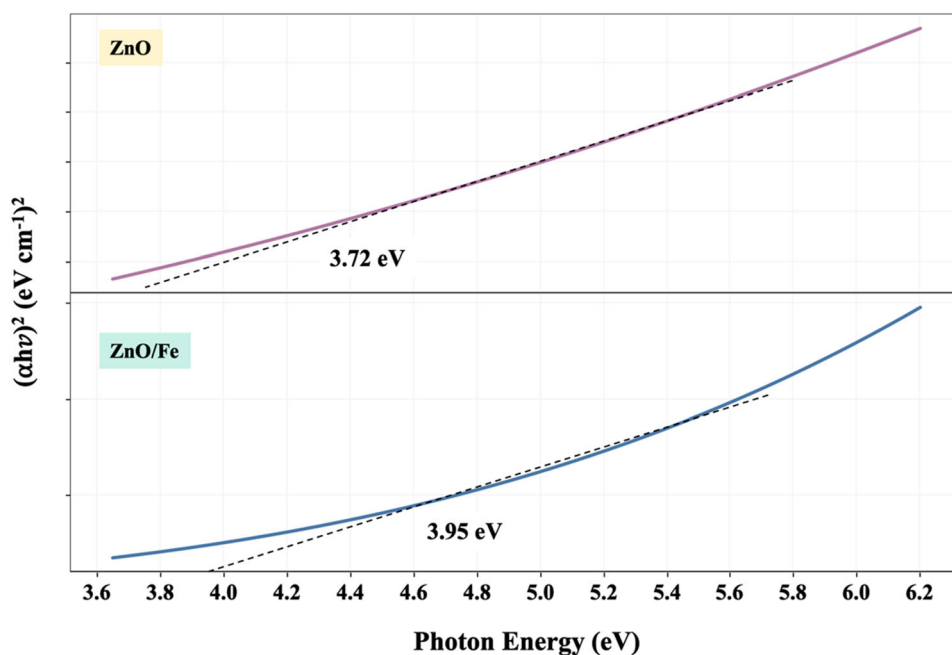
3.6.1 Study of the concentration of the MB dye

The influence of the primary concentrations of the MB dye on the rate of decomposition by the photocatalyst under light and dark conditions (dark conditions) is shown in Table 1 and Fig. 10. Table 1 shows the percentage decolorization efficiency in

100 mL of MB dye solutions under different initial concentrations, namely 10, 20, 30, 40, and 50 mg L^{-1}, of 0.1 ZnO/Fe. It was found that the tendency for the removal of the MB dye showed the same trend under different concentrations for the reactions performed in the presence of light. The removal rate of the MB dye was increased and exhibited the highest dye
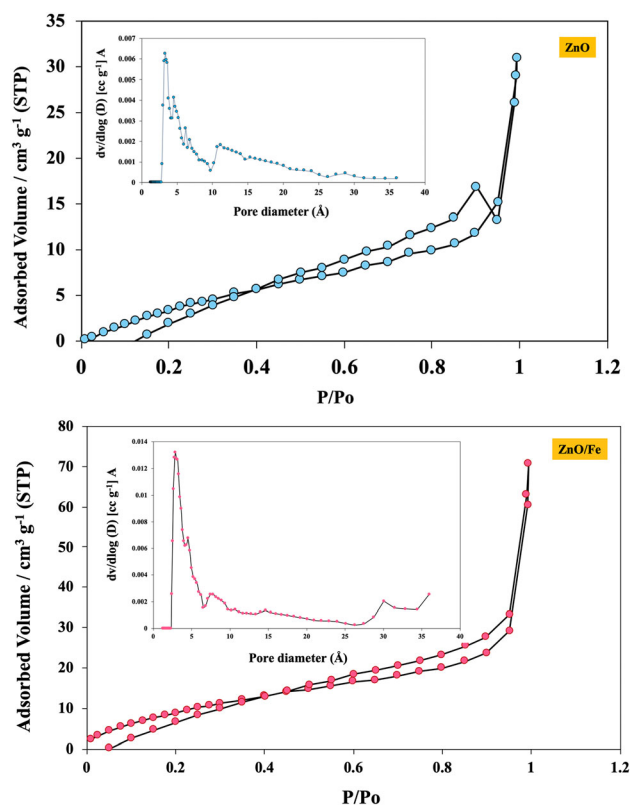
Fig. 8 N$_2$ adsorption–desorption isotherm curve and Pore diameter size (inset) of ZnO and ZnO/Fe photocatalyst

decolorization value at the dye solution concentration of 30 ppm. However, the dye decolorization value was reduced as the concentration of the dye increased to 40 ppm and 50 ppm due to the decrease in the light intensity through the solution. For the reaction performed in the dark, the decrease in the concentration of MB induced the adsorption of the molecules. However, the results showed that the MB adsorption process was less pronounced compared to the photocatalytic decomposition of the dye [25, 26].

3.6.2 Study of the effect of the amount of ZnO/Fe photocatalyst

The effect of the amount of ZnO/Fe photocatalyst on MB dye removal under different catalytic concentrations, namely 0.1, 0.2, 0.3, 0.4, and 0.5 g, in 100 mL of (50 ppm) MB dye solution was studied. The results of the dye removal in the dark and light conditions are shown in Table 2 and Fig. 11. The results indicated an

increase in the decomposition value of the dye as the amount of the photocatalyst rose to 0.4 g. However, the dye decolorization value was found to decrease in the dye solution with a concentration of 50 ppm and 0.5 g of ZnO/Fe due to the excess amount of photocatalyst, resulting in a decrease in the distance between the trapping sites of the electrons and holes [27].

3.6.3 Study of the effect of pH of the MB dye solution

The influence of the initial pH of the solution on the photo-decolorization efficiency for 0.1 g of ZnO/Fe in 10 ppm of MB dye solution was elucidated (Table 3 and Fig. 12). A very high photoactivity was observed under the natural pH of the MB solution (pH 5) in the presence of light. On the contrary, there was a dramatic decrease in photoactivity as the pH lowered to a value of ≈ 3 attributed to the acidic solution. Also, the decolorization efficiency of MB was decreased with the increase in the pH of the MB solution to 9. This is attributed to the high concentration of OH⁻ at high pH values [28]. The negative charge of OH⁻ surrounds the positively charged MB molecule, which reduces the contact between the MB molecules and the photocatalyst, resulting in a lower dye decolorization value.

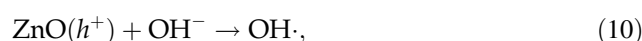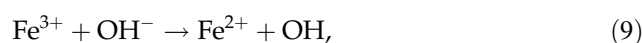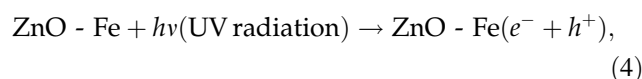### 3.6.4 The stability and recyclability of the ZnO/Fe photocatalyst

The recyclability of the ZnO/Fe photocatalyst was investigated by conducting five consecutive analyzes, whose results are given in Fig. 13. After the initial runs of photocatalytic decolorization, the ZnO/Fe photocatalyst was washed with water, centrifuged, and dried at 110 °C for 3 h. This was followed by the consecutive analytical process. From the results, no remarkable change was observed in the photocatalytic decolorization efficiency of MB above 80% after the three cycles. The recyclability measurements showed that the ZnO/Fe photocatalyst exhibits good reusability and thus finds potential for practical industrial applications.

Fig. 9 Particle size distribution of **a** ZnO and **b** ZnO/Fe photocatalyst
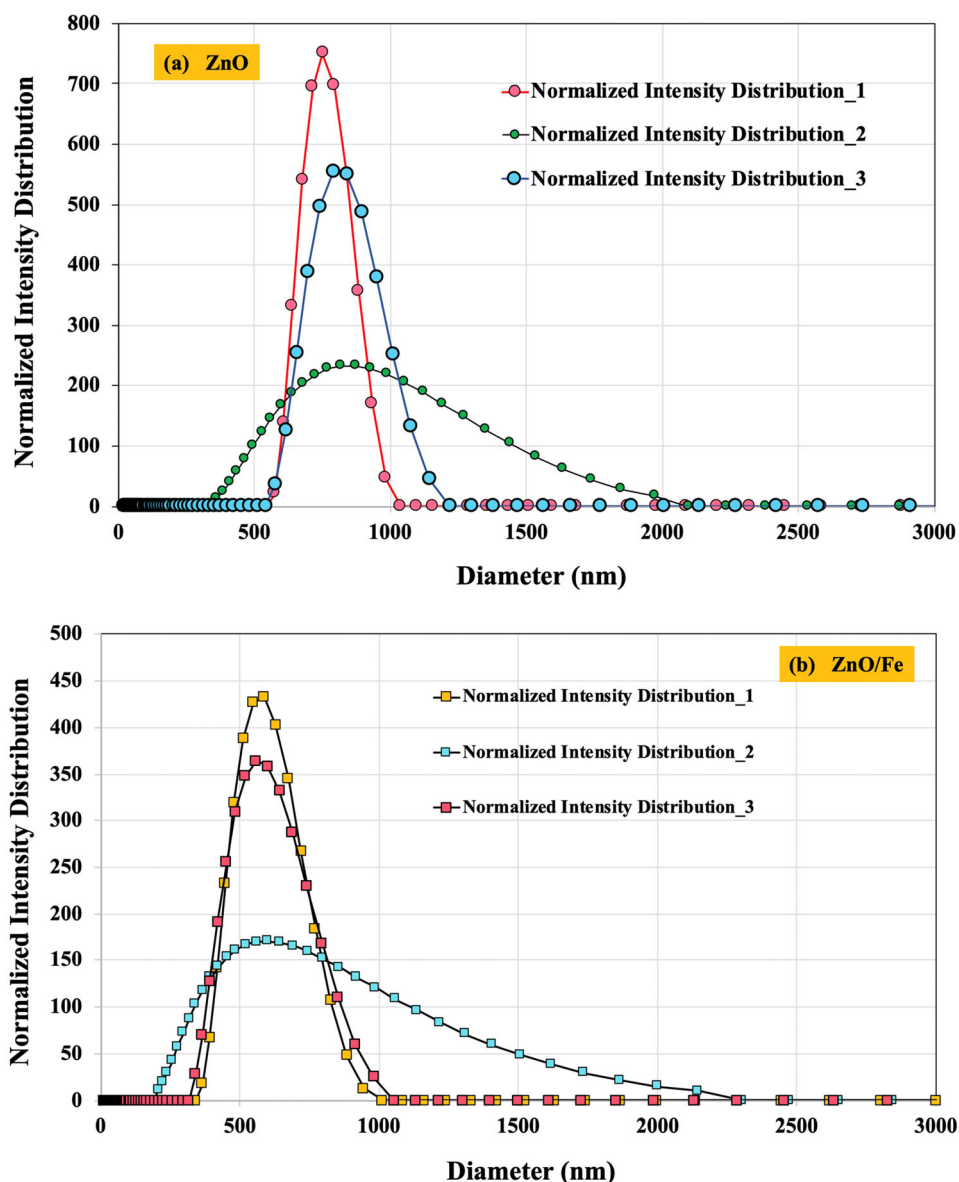
3.6.5 ZnO/Fe photocatalytic mechanism

The effective dye decolorization of MB using ZnO/Fe was observed under UV–Vis light for the photogeneration of electrons and holes. The photogenerated electrons encounter an oxygen molecule to produce superoxide free radicals [29]. The holes react with water and OH⁻ to produce OH•. The production of free radicals was high in the ZnO/Fe photocatalyst compared to the ZnO NPs. On the addition of H_2O_2, the generated superoxide free radicals and hydroxyl free radicals reacted aggressively on the MB dye, resulting in a faster rate of decoloration as shown in Eqs. (4–11) and Fig. 14.

$$ZnO\text{-}Fe + h\nu(\text{UV radiation}) \rightarrow ZnO\text{-}Fe(e^- + h^+), \tag{4}$$

$$Fe^{2+} + (e^-) \rightarrow Fe^+, \tag{5}$$

$$Fe^+ + O_2 \rightarrow Fe^{2+} + O_2^-, \tag{6}$$

$$ZnO(e^-) + O_2 \rightarrow O^{2-}, \tag{7}$$

$$Fe^{2+}(ZnO) + h^+ \rightarrow Fe^{3+}, \tag{8}$$

$$Fe^{3+} + OH^- \rightarrow Fe^{2+} + OH, \tag{9}$$

$$ZnO(h^+) + OH^- \rightarrow OH\cdot, \tag{10}$$

$$(\text{Added})H_2O_2 + (e^-) \rightarrow OH + OH^-. \tag{11}$$

Table 1 Percentage of MB decolorization under different initial dye concentrations in the light and dark conditions

Time (*t*)	% Dye removal efficiency for light conditions with difference initial concentration				
	10 mg L^{-1}	20 mg L^{-1}	30 mg L^{-1}	40 mg L^{-1}	50 mg L^{-1}
0	0	0	0	0	0
5	12.18	4.82	6.44	3.97	2.20
10	26.38	14.18	17.82	12.00	7.76
15	41.14	22.02	26.21	17.48	13.00
20	62.28	34.32	36.38	23.7	18.54
25	84.14	48.38	46.64	31.62	25.10
30	98.16	65.08	59.61	39.10	30.44

Time (*t*)	% Dye removal efficiency for dark conditions with difference initial concentration				
	10 mg L^{-1}	20 mg L^{-1}	30 mg L^{-1}	40 mg L^{-1}	50 mg L^{-1}
0	0	0	0	0	0
5	3.24	2.88	2.24	1.88	2.45
10	2.26	3.08	2.24	2.61	2.95
15	4.44	3.70	2.95	3.09	3.97
20	6.04	4.75	3.67	4.85	4.70
25	11.70	7.23	5.80	5.29	6.79
30	20.76	11.75	8.47	7.93	7.40

Fig. 10 Decolorization of MB using the ZnO/Fe photocatalysts according to the relative concentration (C_t/C_0) of the MB dye versus concentration of the MB solution in the light and dark conditions
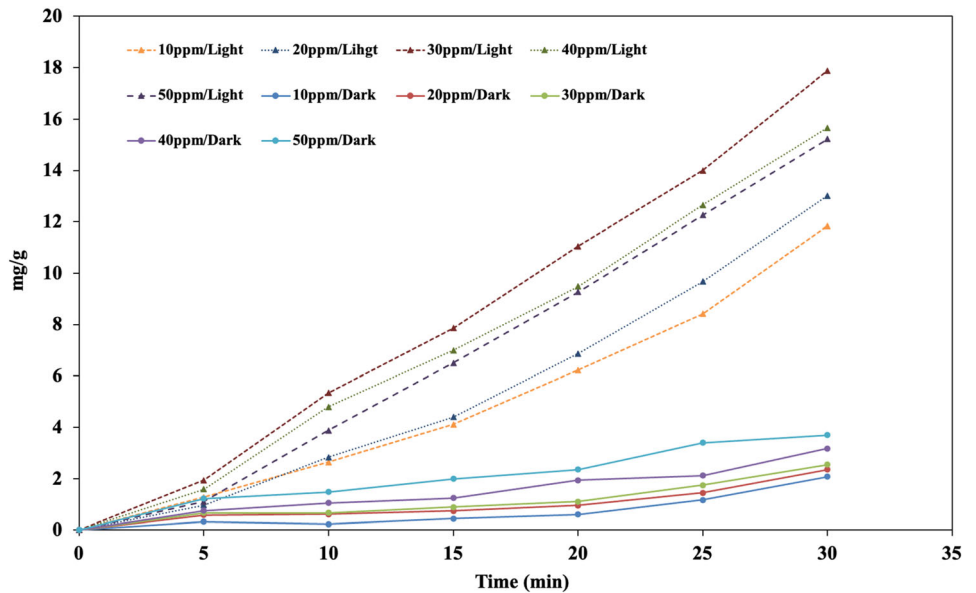
All the radical groups reacted with the dye molecules to cause a highly efficient decolorization of the methylene blue dye along with the formation of by-products.

4 Conclusion

A simple and economical microwave method was successfully devised for the fabrication of a ZnO/Fe photocatalyst. The developed ZnO/Fe photocatalyst exhibited better performance with regard to the

Table 2 Percentage of MB decolorization under various amounts of the ZnO/Fe photocatalyst in light and dark conditions

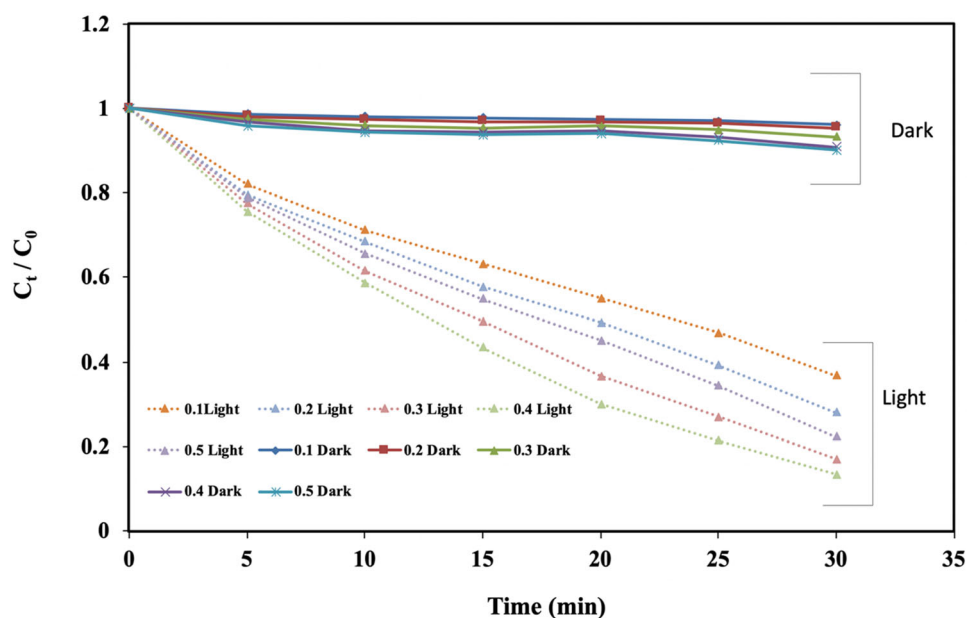| Time (t)	% Dye removal efficiency for light conditions with difference ZnO/Fe photocatalyst amount				
	0.1 g	0.2 g	0.3 g	0.4 g	0.5 g
0	0	0	0	0	0
5	17.9	20.4	22.4	24.4	21.1
10	28.7	31.5	38.4	41.3	34.4
15	36.8	42.2	50.4	56.5	45.1
20	44.9	50.6	63.3	69.9	54.9
25	53.0	60.8	72.9	78.6	65.6
30	63.2	71.9	83.0	86.5	77.6
Time (t)	% Dye removal efficiency for dark conditions with difference ZnO/Fe photocatalyst amount				
	0.1 g	0.2 g	0.3 g	0.4 g	0.5 g
0	0	0	0	0	0
5	1.3	1.9	2.5	3.3	4.1
10	1.9	2.6	4.0	5.2	5.7
15	2.2	3.1	4.6	5.6	6.3
20	2.7	3.1	4.2	5.3	6.0
25	2.9	3.5	5.1	6.9	7.7
30	3.9	4.6	6.7	9.1	9.9

Fig. 11 Decolorization of MB using the ZnO/Fe photocatalysts according to the relative concentration (C_t/C_0) of the MB dye versus the amount of photocatalysts in the light and dark conditions

photo-decolorization of MB relative to pure ZnO. The wide band gap of ZnO was decreased by the presence of Fe. Therefore, the decolorization rate of MB increased with the decrease in the band gap energy. The factors affecting the phototropic process of the elimination of MB dye solution were studied under

Table 3 Percentage of MB decolorization under different pH values of the dye solutions in the light and dark conditions

| Time (*t*)	% Dye removal efficiency for light conditions with difference ZnO/Fe photocatalyst amount				
	pH 3	pH 5	pH 6.63 (initial)	pH 7	pH 9
0	0.0	0.0	0	0	0
5	46.7	49.0	47.3	46.6	35.9
10	70.7	68.8	66.6	66.4	52
15	88.2	85.3	81.4	84.6	67.2
20	95.8	93.9	93.9	90.6	79.8
25	98.3	98.4	97.1	97.7	84.4
30	98.6	99.1	98.6	97.9	86.3
Time (*t*)	% Dye removal efficiency for dark conditions with difference ZnO/Fe photocatalyst amount				
	pH 3	pH 5	pH 6.63 (initial)	pH 7	pH 9
0	0	0	0	0	0
5	5.3	7.8	7.1	3.5	2.8
10	5.7	8.0	7.2	4.2	3.6
15	5.7	8.0	6.6	4.0	2.5
20	5.0	9.9	8.5	3.5	3.0
25	5.6	10.5	7.8	4.0	2.5
30	5.8	12.0	9.9	5.0	3.8

Fig. 12 Decolorization of MB using the ZnO/Fe photocatalysts according to the relative concentration (C_t/C_0) of the MB dye versus pH of the MB solutions in the light and dark conditions
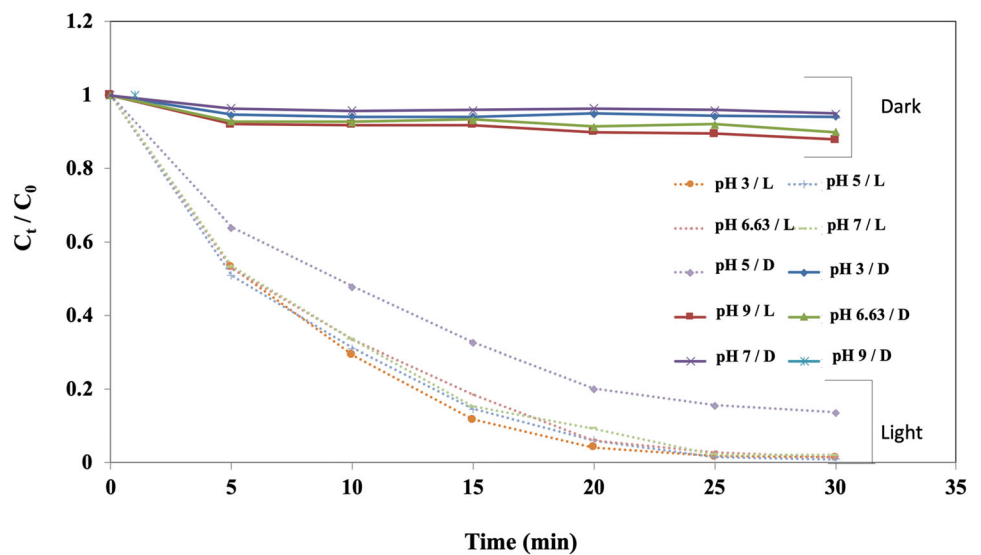
visible light. The highest decolorization efficiency of MB dye was observed at the reaction time of 30 min under the dye concentration of 300 ppm using 0.4 g of the catalyst and pH value in the range of 3–7, causing the decolorization of more than 85% of the initial dye concentration. On recycling the photocatalyst, the decomposition value of the dye was found to decrease with the number of reuse cycles. However, there was only a slight reduction in the decolorization value. Also, the dye removal value was 80% during the third recycling trial. As a result, this photocatalyst finds potential application in the decolorization of the dye from industrial pollutants due to its fast, practical, and highly efficient dye removal process.

Fig. 13 The stability and recyclability of the ZnO/Fe photocatalyst
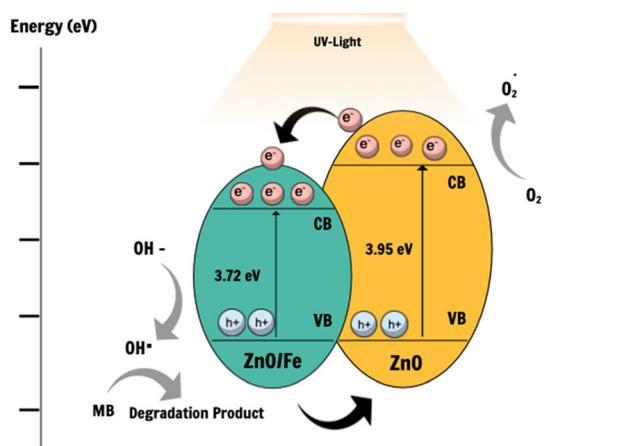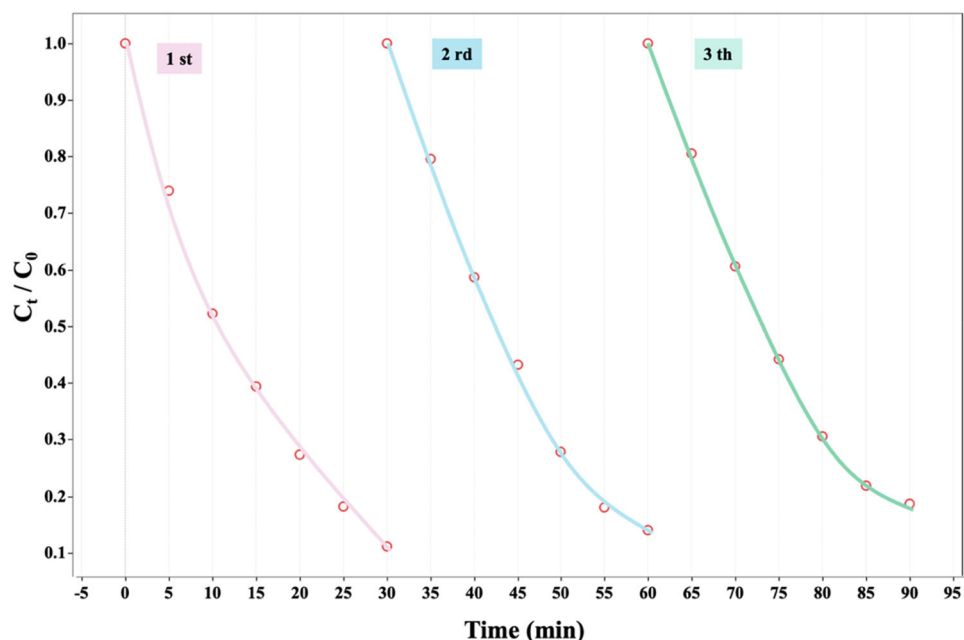
Fig. 14 Schematic illustration of the electron–hole pairs separation and migration between ZnO and ZnO/Fe under visible light irradiation

Acknowledgements

Funding

Declarations

Conflict of interest The authors have not disclosed any conflict of interest.

References

1. S.V. Manjunath, B.K. Tripathy, M. Kumar, S. Pramod, J. Environ. Chem. Eng. **8**, 104486 (2020)
2. A. Hou, H. Chen, Y. Xu, X. Yang, Y. Zhang, K. Xie, A. Gao, J. Cleaner Prod. **274**, 122935 (2020)
3. A.Q. Alorabi, M.S. Hassan, M. Azizi, Arabian J. Chem. **13**, 8080–8091 (2020)
4. Y. Sun, P. Meng, X. Liu, Appl. Surf. Sci. **456**, 259–269 (2018)
5. Y. Areerob, K.Y. Cho, W.C. Oh, J. Photochem. Photobiol. A **340**, 157–169 (2017)
6. Z. Zafar, R. Fatima, J.O. Kim, Environ. Res. **197**, 111120 (2021)
7. M.A. Majeed Khan, S. Kumar, A.N. Alhazaa, M.A. Al-Gawati, Mater. Sci. Semicond. Process. **87**, 134–141 (2018)
8. M.A. Majeed Khan, R. Siwach, S. Kumar, M. Ahmed, J. Ahmed, J Mater Sci **31**, 6360–6371 (2020)
9. M.A. Majeed Khan, R. Siwach, S. Kumar, M. Ahamed, J. Ahmed, J. Alloys Compd. **856**, 158127 (2020)
10. P. Hemalatha, S.N. Karthick, K.V. Hemalatha, M. Yi, H.J. Kim, M. Alagar, J. Mater. Sci. **27**, 2367–2378 (2016)
11. A. Modwi, M.A. Ghanem, J. Mol. Struct. **1173**, 1–6 (2018)
12. S. Selvaraj, M.K. Mohan, M. Navaneethana, S. Ponnusamy, C. Muthamizhchelvan, Mater. Sci. Semicond. Process. **103**, 104622 (2019)

13. X. Zhang, W.F. Chen, G. Bahmanrokh, V. Kumar, N. Ho, P. Koshy, C.C. Sorrell, Nano-Struct. Nano-Objects **24**, 100557 (2020)

14. S. Castro-Lopes, Y. Guerra, A. Silva-Sousa, D.M. Oliveira, L.A.P. Gonçalves, A. Franco, E. Padron-Hernandez, R. Pena-Garcia, Solid State Sci. **109**, 106438 (2020)

15. H.R. Khan, M. Aamir, B. Akramd, A.A. Tahir, M.A. Malik, M.A. Choudhary, J. Akhtar, Mater. Res. Bull. **122**, 110627 (2020)

16. H. Khan, M. Habib, A. Khan, D.C. Boffito, J. Environ. Chem. Eng. **8**, 104282 (2020)

17. A.P. Torane, A.B. Ubale, K.G. Kanade, P.K. Pagare, Mater. Today **43**, 2738–2741 (2021)

18. H. Jiang, X. Zhang, W. Gu, X. Feng, L. Zhang, Y. Weng, Chem. Phys. Lett. **711**, 100–106 (2018)

19. H. Wanga, M. Cao, C. Tao, H. Hao, Z. Yao, H. Liu, J. Alloys Compd. **864**, 158644 (2021)

20. N. Aggarwal, K. Kaur, A. Vasishth, N.K. Verma, J. Mater. Sci. Mater. Electron. **27**, 13006–13011 (2016)

21. C. Guo, K. Tian, L. Wang, F. Liang, F. Wang, D. Chen, J. Ning, Y. Zhong, Y. Hu, J. Colloid Interface Sci. **583**, 661–671 (2021)

22. C. Venkatareddy, N. Bandaru, I.N. Reddy, J. Shim, K. Yoo, Mater. Sci. Eng. B **232**, 68–75 (2018)

23. M.A. Majeed Khan, S. Kumar, M. Ahamed, S.A. Alrokayan, J. Mater. Sci. **26**, 6113–6118 (2015)

24. H. Ullah, M.B. Vishlaghi, T. Balkan, Z. Rehman, S. Kaya, Inorg. Chem. Commun. **130**, 108744 (2021)

25. L. Liu, Z. Liu, Y. Yang, M. Geng, Y. Zou, M.B. Shahzad, Y. Daia, Ceram. Int. **44**, 19998–20005 (2018)

26. Y. Wang, X. Zhang, C. Hou, Nano-Struct. Nano-Objects **16**, 250–257 (2018)

27. F. Heshmatpour, M.S. Abdikhani, Phys. B **570**, 312–319 (2019)

28. M. Naghizadeh, M.A. Taher, A.M. Tamaddon, Heliyon **5**, 02870 (2019)

29. H.M. Lwin, W. Zhan, S. Song, F. Jia, J. Zhou, Chem. Phys. Lett. **736**, 136806 (2019)